Design and Operational Analysis of Amphibious Aircraft

Prof. Ranjith Mohan
Parikshit Sonwane AE22B042, Devang Patwardhan AE22B043

Department of Aerospace Engineering
Indian Institute of Technology Madras, Chennai

Date of Submission: 02.05.2025

This report analyzes a hybrid aerial vehicle designed for operation in both air and water. The study evaluates various airfoil profiles to optimize configurations for a vertical takeoff and landing prototype. Aerodynamic and hydrodynamic simulations identify suitable airfoil types, speeds, and propulsion systems for dual-medium performance. The findings highlight airfoils that maintain efficiency across both environments, with recommended operating parameters and propeller specifications.

1 Introduction

Amphibious aircraft, capable of operating seamlessly on both land and water, represent a unique class of aviation technology that addresses a wide range of logistical and operational challenges. These aircraft offer significant strategic advantages in regions with limited runway infrastructure or extensive water networks, supporting activities such as search and rescue, surveillance, environmental monitoring, and passenger transport.

Designing an effective amphibious aircraft requires balancing aerodynamic efficiency in flight with hydrodynamic stability during water operations. This dual requirement presents complex challenges in airframe configuration, airfoil selection, and propulsion integration. While traditional amphibious designs primarily focus on structural adaptations such as hull shapes and retractable landing gear, optimizing aerodynamic surfaces for performance in both air and water environments remains a critical area of development.

This study focuses on the evaluation of various airfoil profiles and the determination of operating parameters suited for a prototype amphibious aircraft featuring vertical takeoff and landing (VTOL) capabilities. Using aerodynamic and hydrodynamic simulations, the analysis identifies optimal airfoil types, operational speeds, and propulsion characteristics necessary for efficient dual-medium performance.

The structure of this report is as follows: Section III explains the theory behind designing an aircraft. Section IV outlines the methodology and simulation framework. Section V presents the aerodynamic and hydrodynamic analysis results. Sections VI and VII outline the propeller designs. Finally, Section VIII concludes the report with key conclusions.

2 Literature Review

The design of amphibious aircraft requires a balance between aerodynamic efficiency in air and hydrodynamic stability in water. Previous studies highlight the importance of selecting airfoils with high lift-to-drag ratios and stable stall characteristics, such as NACA 4412, Clark Y, and Eppler profiles, to ensure efficient performance across both mediums.

Hydrodynamic research emphasizes the need for low-drag, high-lift airfoils to maintain stability during submerged operation, especially at low Reynolds numbers. Similarly, propeller design must account for the drastic differences in air and water densities, optimizing parameters like solidity ratio, thrust coefficient, and advance ratio for each environment.

While traditional amphibious designs often prioritize one medium, achieving true dual-environment optimization remains a developing area. This project extends previous work by systematically analyzing airfoils, wing geometries, and propeller configurations for efficient operation in both air and water.

3 Concept

This section outlines the theoretical framework guiding the aerodynamic, structural, and hydrodynamic design of the prototype, covering critical concepts such as airfoil selection, wing and propeller performance estimation, and transition dynamics between air and water.

3.1 Airfoil Understanding and Selection

3.1.1 Understanding Airfoils

Airfoils are fundamental to the aerodynamic behavior of aircraft, directly influencing lift, drag, pitching moments, and stall characteristics. Their careful selection is critical for achieving the desired flight performance, particularly in applications requiring efficient operation in multiple

environments such as air and water.

Key aerodynamic parameters defining airfoil behavior include the lift coefficient (C_L), drag coefficient (C_D), and pitching moment coefficient (C_m). The stall behavior, whether abrupt or gradual, significantly affects stability and controllability. Cambered airfoils generate higher lift at the cost of increased pitching moments, while symmetric airfoils, possessing zero camber, are favored for applications requiring balanced inverted and upright flight performance.

Airfoil thickness plays an important role in structural considerations; thicker airfoils permit stronger yet lightweight wing constructions but may lead to increased drag. Furthermore, the Reynolds number (Re) profoundly impacts airfoil performance, with lower Re values typical of small-scale aircraft resulting in higher drag and earlier stall onset compared to full-scale counterparts.

Laminar flow airfoils, designed to maintain extensive laminar boundary layers, offer lower drag but are sensitive to surface contamination and turbulence, making them less forgiving under operational conditions involving rough surfaces or water exposure.

3.1.2 Airfoil Selection

The selection of an appropriate airfoil requires balancing several competing factors, including mission profile, desired flight characteristics, and structural constraints. High-lift airfoils are advantageous for low-speed, short takeoff and landing (STOL) operations, making them suitable for amphibious aircraft designs. Symmetric airfoils, on the other hand, are commonly employed in aerobatic applications due to their neutral lift at zero angle of attack.

Airfoils exhibiting gentle stall behavior, such as the Eppler E197, are preferred for designs prioritizing stability and predictable handling. The pitching moment characteristics must also be considered, as highly negative pitching moments can impose greater structural loads and necessitate higher trim forces, adversely impacting efficiency.

Operational Reynolds number ranges dictate the appropriate airfoil choice, as performance characteristics such as lift-to-drag ratio (C_L/C_D) vary significantly with scale and speed. Consequently, airfoils must be selected to perform optimally within the expected flight envelope.

Commonly employed airfoils include the Eppler E197, noted for its moderate camber and forgiving stall behavior; the Clark Y, valued for its simplicity and stable performance; and the NACA 4412, which offers strong low-speed lift capabilities, making it well-suited for general-purpose and amphibious operations.

The final airfoil selection reflects a compromise between aerodynamic efficiency, structural integrity, and operational versatility, ensuring reliable performance across both aerial and aquatic environments.

3.2 Wing Design and Performance Estimation

3.2.1 Wing Loading

Wing loading is a critical parameter in aircraft design, defined as the ratio of an aircraft's gross weight to its wing area, typically expressed in ounces per square foot. It directly influences stall speed, maneuverability, structural strength requirements, and landing characteristics.

Higher wing loading generally results in smaller, stronger, and faster aircraft, but leads to higher stall and landing speeds. Conversely, lower wing loading favors slower, more forgiving flight behavior, which is advantageous for training aircraft and amphibious designs.

The required wing area (A) can be determined once the gross weight (W) and the desired wing loading (WL) are specified, using the following expression:

$$A = \frac{W}{WL} \tag{1}$$

where A is in square metres, W is in kilograns, and WL is in kg/m^2.

The estimated landing speed is closely linked to stall speed, which is determined based on the maximum lift coefficient (C_L) and includes an added safety margin.

3.2.2 Wing Structural Considerations

In the structural design process, the aircraft's total weight is divided between fixed-weight components (such as engines, control systems, and landing gear) and variable-weight components (such as wings, fuselage, and tail surfaces). Typically, over 50% of the gross weight belongs to fixed components.

Key observations regarding structural design include:

- Higher wing loading permits lighter wing structures, as lower structural margins are required.
- Larger wing areas reduce stall speeds but increase drag, which can negatively affect top speed and efficiency.

An optimized wing design must therefore achieve a careful balance between structural lightness and aerodynamic efficiency.

3.2.3 Center of Gravity (CG) Location and Balancing

Correct placement of the center of gravity (CG) is essential for ensuring longitudinal stability and controllability. During the design phase, a "balancing act" approach can be employed:

- Draw the aircraft's side view and locate the CGs of all major components.
- Use a simulated balance beam setup to predict the overall CG position.
- Adjust component placement: moving the engine or battery forward if the aircraft is tail-heavy, or moving the wing forward if it is nose-heavy.

Ideally, the CG should be positioned slightly forward of the aircraft's neutral point (NP) to ensure a positive static margin and stable flight behavior.

Failure to achieve proper balancing can result in flight instability, poor handling, and increased control forces, negatively impacting overall aircraft performance.

3.3 Propeller Design and Performance Estimation

3.3.1 Propeller Fundamentals

A propeller functions similarly to a rotating wing, producing thrust by accelerating a mass of air rearward. It is characterized primarily by two parameters: diameter and pitch, both of which influence thrust generation and flight speed.

The diameter determines the area of air affected, while the pitch represents the theoretical distance (in meters) the propeller would advance in one revolution in an ideal, slip-free condition.

High-speed aircraft generally favor smaller diameters and higher pitch values, while low-speed, high-thrust applications benefit from larger diameters and lower pitch settings.

3.3.2 Nominal and Effective Pitch

The *nominal pitch* is the geometric pitch measured at approximately 75% of the propeller blade's radius. However, the *effective pitch* accounts for aerodynamic slip and real-world inefficiencies, and thus represents the actual distance advanced per revolution under load.

Propeller slip can be estimated by comparing the theoretical pitch-based advance to the actual forward distance traveled per revolution.

3.3.3 Estimating Level Flight Speeds

In level flight, the speed of the aircraft (V) can be approximated using the propeller pitch (P) and the operating rotational speed (in revolutions per second, RPS) as:

$$V = P \times n \times \eta \tag{2}$$

where:

- V is the flight speed (m/s),
- P is the effective pitch (m),
- n is the propeller rotational speed (revolutions per second),
- η is the propeller efficiency (typically between 0.7 and 0.85).

The propeller efficiency η accounts for slip and other aerodynamic losses.
Thus, the speed in terms of RPM becomes:

$$V = P \times \frac{\text{RPM}}{60} \times \eta \tag{3}$$

3.3.4 Propeller Material Considerations

Propellers are manufactured from various materials including wood, nylon composites, and fiber-reinforced plastics. Reinforced plastic propellers are preferred for high-load applications due to their structural rigidity and resistance to deformation.

Ensuring accurate propeller balancing is critical to minimize vibrations, which can otherwise lead to structural fatigue and decreased propulsion efficiency.

3.4 Transition Between Air and Water

The transition phase between waterborne and airborne operation represents a critical aspect of amphibious aircraft performance. During water takeoff and landing, the vehicle is subjected to a combination of hydrodynamic and aerodynamic forces that must be managed carefully to ensure stability, efficiency, and structural integrity.

At low speeds, hydrodynamic forces dominate due to the significantly higher density of water compared to air. The aircraft must overcome substantial water drag while generating sufficient hydrodynamic lift to progressively reduce wetted area and resistance. As speed increases, aerodynamic lift produced by the wings becomes comparable to hydrodynamic lift, enabling the aircraft to achieve a smooth transition into flight.

Key challenges during the transition include:

- **High Hydrodynamic Drag:** The initial acceleration phase demands high thrust to overcome water resistance.
- **Dynamic Pitching Moments:** Shifting centers of pressure can induce pitching instabilities requiring corrective control inputs.
- **Spray Interference:** Water spray can impact propeller performance and impose additional structural loads on lower surfaces.
- **Porpoising Instabilities:** Improper balancing can lead to oscillatory motions during planing, which must be mitigated through careful CG positioning and hull design.

Design strategies to facilitate smooth transition include optimizing hull or float shapes to enhance hydrodynamic

lift, maintaining the center of gravity (CG) forward of the aerodynamic neutral point to ensure positive static margin, and selecting wing incidence angles that allow for early lift-off at moderate speeds without excessive rotation.

4 Design Methodology

The design methodology followed a systematic sequence involving airfoil analysis, wing design, and aerodynamic-hydrodynamic performance evaluation for the amphibious aircraft prototype.

4.1 Airfoil Analysis

Initially, multiple airfoil profiles were analyzed to determine their suitability for dual-medium operation. The chord length was fixed at 0.3 meters. Each airfoil was evaluated over a range of Reynolds numbers by generating the following plots:

- Lift coefficient (C_L) vs. angle of attack (α),
- Drag coefficient (C_D) vs. angle of attack (α),
- Moment coefficient (C_m) vs. angle of attack (α),
- Lift-to-drag ratio (C_L/C_D) vs. lift coefficient (C_L).

Based on the comparative analysis of these plots, airfoils demonstrating favorable lift, low drag, and high aerodynamic efficiency were shortlisted for further study.

4.2 Wing Design

A wing was designed based on the selected airfoils. Key geometric parameters, shown in Table 1, were optimized to achieve the desired performance in both air and water environments.

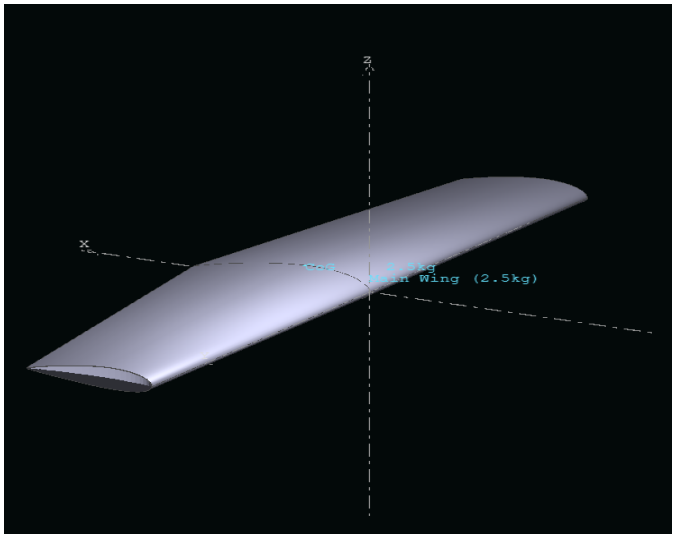

Figure 1: Wing geometry used for analysis.

Table 1: Wing Geometry Parameters

Parameter	Value
Wing Span	1.5 m
XY Projected Span	1.5 m
Wing Area	0.45 m^2
Projected Area	0.45 m^2
Root Chord	0.350 m
Mean Aerodynamic Chord (MAC)	0.303 m
Tip Twist	0.000°
Aspect Ratio	5.000
Taper Ratio	0.714
Root-Tip Sweep	−1.909°
Dihedral Angle	0.000°

4.3 Operating Weight Considerations

Operating weights were defined separately for aerial and aquatic conditions:

- Airborne Mode: 2.5 kg (gross weight),
- Waterborne Mode: 1.75 kg (considering buoyancy and weight distribution effects).

These weights were used as inputs for aerodynamic and hydrodynamic performance analysis.

4.4 Performance Analysis

Further analysis involved evaluating the designed wing and selected airfoils under realistic operating conditions for both air and water environments. The following performance parameters were studied:

- Drag force (F_x) vs. velocity (V_x) to identify optimal operating speeds (corresponding to minimum drag conditions),
- Lift coefficient (C_L) vs. angle of attack (α),
- Drag coefficient (C_D) vs. angle of attack (α),
- Lift-to-drag ratio (C_L/C_D) vs. angle of attack (α) to determine efficiency at standard operating angles,
- Lift-to-drag ratio (C_L/C_D) vs. lift coefficient (C_L) to identify the peak efficiency point,
- Cruise velocity (V_x) vs. angle of attack (α) relationships.

Separate analyses were performed for air and water to account for differences in fluid density and dynamic forces.

4.5 VLM2 Analysis

For the analysis, the VLM2 (Vortex Lattice Method 2) was used. It models the wing with bound vortices to estimate lift and induced drag, offering a fast and reliable first-order prediction by assuming inviscid, attached flow and neglecting viscous effects.

4.6 Propeller Selection and Operational Analysis

A two-blade propeller configuration was selected for the prototype, considering its structural simplicity, reduced weight, and lower parasitic drag compared to multi-blade systems. Two-blade designs also offer higher efficiency at moderate thrust requirements, making them suitable for the operating speeds targeted in both aerial and aquatic environments.

Propeller sizing and performance estimation were conducted based on the aerodynamic and hydrodynamic performance results obtained previously. Specifically, the drag force (F_x) vs. cruise velocity (V_x) graphs were analyzed to identify the low-drag operating conditions.

Once the optimal velocity ranges were determined from the F_x vs V_x curves, the following procedure was applied:

- **Rotational Speed (ω) Calculation:** The required rotational speed of the propeller shaft (ω in rad/s) was computed to match the identified velocity and thrust conditions.
- **Advance Ratio (J) Calculation:** The advance ratio J was calculated using:

$$J = \frac{V}{nD} \tag{4}$$

  where:

  - V is the cruise velocity (m/s),
  - n is the rotational speed in revolutions per second,
  - D is the propeller diameter (m).

- **Propeller Efficiency Estimation:** Using empirical charts and advance ratio values, the propeller efficiency (η_p) was estimated. Efficiency values were cross-verified with expected performance ranges for small-scale two-blade propellers.

5 Aero-Hydrodynamic Analysis

5.1 Airfoil Aerodynamic Characteristics

Five airfoils Eppler, Selig1223, Clark Y, NACA4412, and NACA2421 were analyzed over varying Reynolds numbers[1].

5.1.1 Lift Coefficient (C_l) vs Angle of Attack (α)

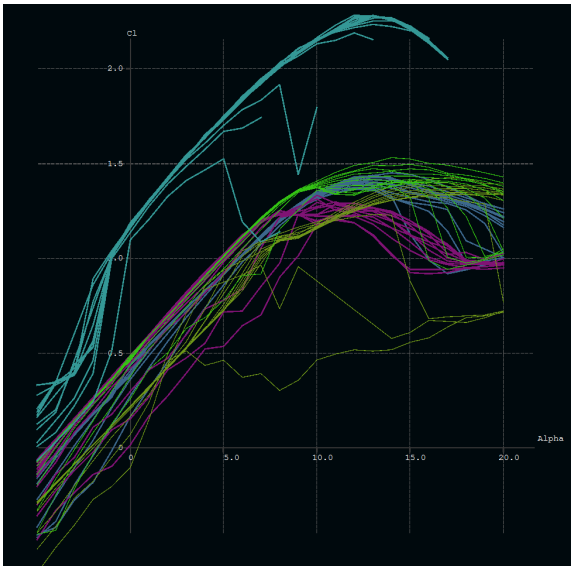

Figure 2: Lift coefficient (C_l) vs. angle of attack (α)

NACA 4412 exhibited the highest maximum lift coefficient with smooth stall, while Clark Y and NACA 2421 showed moderate lift. Eppler provided stable performance across a wide range of angles, and Selig 1223 had a sharp lift increase but tended to stall earlier.

5.1.2 Drag Coefficient (C_d) vs Angle of Attack (α)

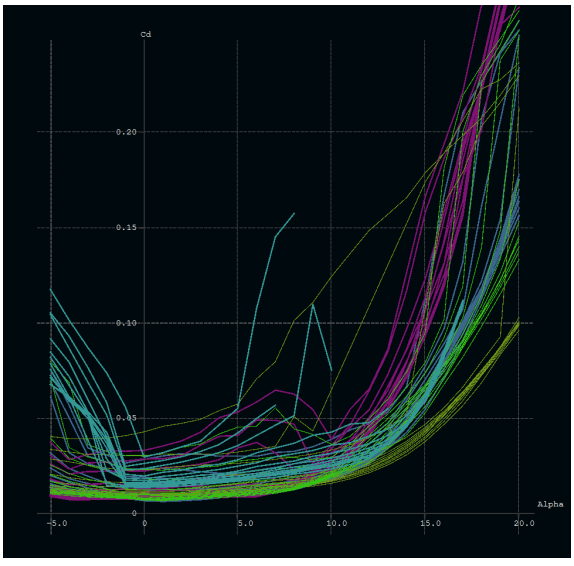

Figure 3: Drag coefficient (C_d) vs. angle of attack (α)

Eppler and NACA 4412 maintained low drag at moderate angles of attack. Selig 1223 experienced higher drag growth at larger α, while Clark Y presented a rapid drag increase beyond stall onset.

5.1.3 Lift Coefficient (C_l) vs Drag Coefficient (C_d)

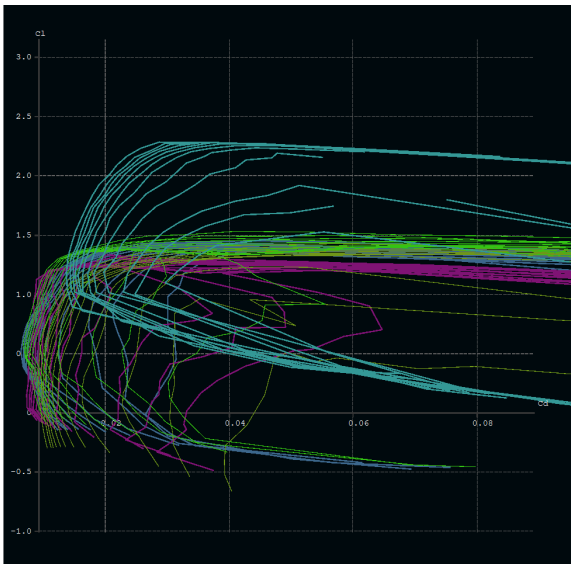

Figure 4: Lift coefficient (C_l) vs. drag coefficient (C_d)

The C_l vs C_d curves confirmed that NACA 4412, Clark Y, and Eppler achieved higher aerodynamic efficiency compared to Selig 1223, which demonstrated relatively higher drag for the same lift.

5.1.4 Moment Coefficient (C_m) vs Angle of Attack (α)

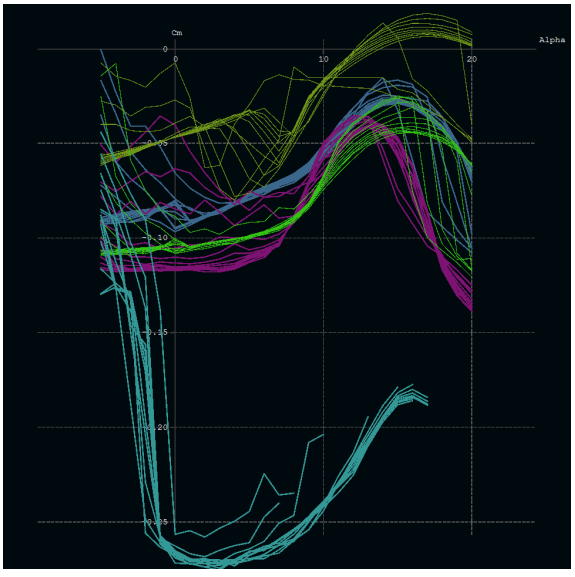

Figure 5: Moment coefficient (C_m) vs. angle of attack (α)

Eppler and NACA 4412 exhibited stable moment curves with favorable pitch stability. Clark Y maintained moderate stability, while Selig 1223 showed larger variations, indicating reduced longitudinal stability.

5.1.5 Lift-to-Drag Ratio (C_L/C_D) vs Angle of Attack (α) at $Re = 3 \times 10^5$

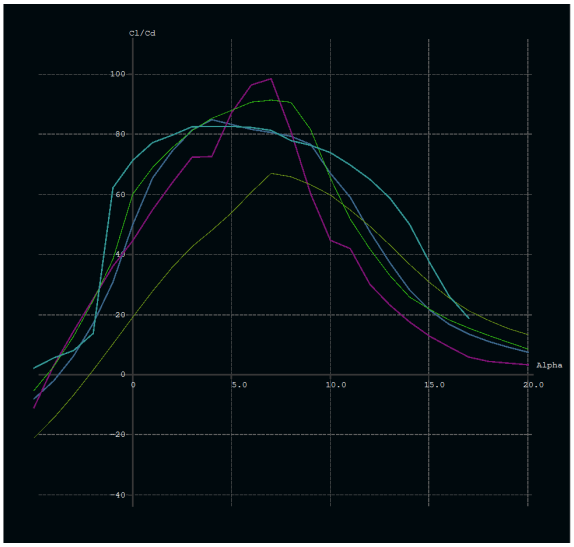

Figure 6: Lift-to-drag ratio (C_L/C_D) vs. angle of attack (α) at $Re = 3 \times 10^5$

Peak aerodynamic efficiency occurred between 4° and 6° angle of attack. Eppler achieved the highest C_L/C_D values, closely followed by NACA 4412 and Clark Y.

5.1.6 Summary

Based on the comparative aerodynamic analysis:

- **Recommended Airfoils**: NACA 4412, Eppler, and Clark Y.
- **Operating Speeds**: Optimal between 10–20 m/s.
- **Efficiency Range**: Maximum lift-to-drag ratio achieved near 4°–6° angle of attack.

[1]The airfoils are represented by the following colors: Eppler in magenta, Selig 1223 in cyan, Clark Y in blue, NACA 4412 in green, and NACA 2421 in olive.

5.2 Wing Aerodynamic Performance in Air

5.2.1 Drag Force (F_X) vs Velocity (V_X)

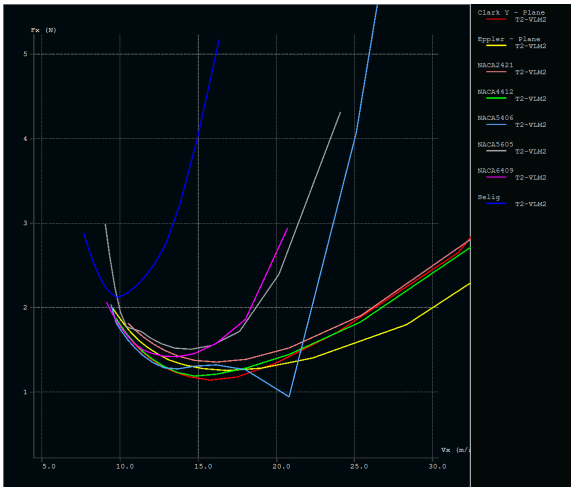

Figure 7: Air: Drag force (F_x) vs. cruise velocity (V_x)

NACA 4412, Clark Y, and Eppler exhibited consistently lower drag forces across the velocity range ($5 - 25m/s$), with optimal performance observed at $15m/s$. Selig 1223 demonstrated significantly higher drag, particularly at increased velocities.

5.2.2 Lift-to-Drag Ratio (C_L/C_D) vs Lift Coefficient (C_L)

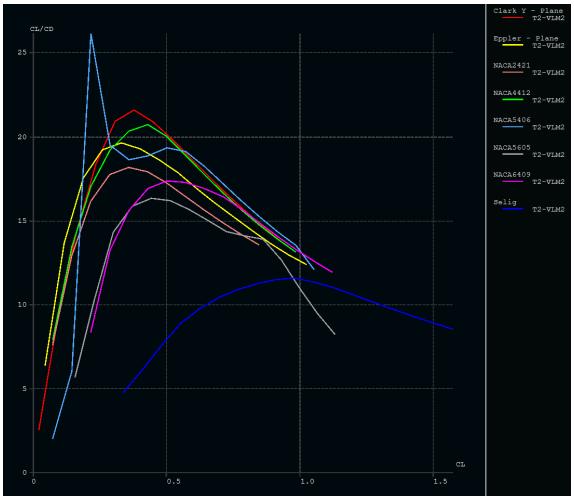

Figure 8: Air: Lift-to-drag ratio (C_L/C_D) vs. lift coefficient (C_L)

The analysis revealed peak efficiency for NACA 4412 and Eppler ($C_L/C_D \approx 22$) at moderate lift coefficients ($0.4 - 0.6$). Clark Y showed slightly reduced performance ($C_L/C_D \approx 20$), while Selig 1223 exhibited substantially lower efficiency across all C_L values.

5.2.3 Lift-to-Drag Ratio (C_L/C_D) vs Angle of Attack (α)

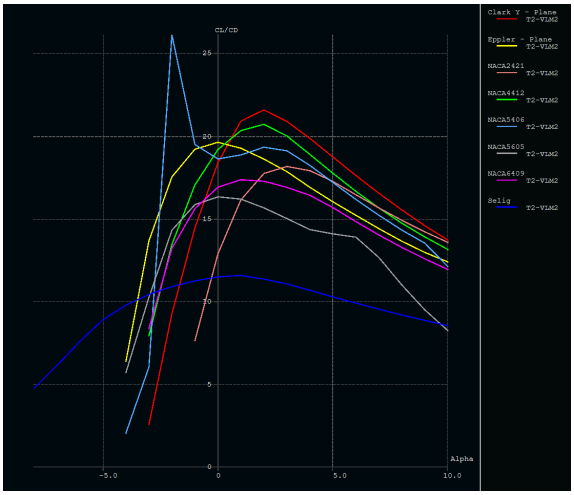

Figure 9: Air: Lift-to-drag ratio (C_L/C_D) vs. angle of attack (α)

Maximum aerodynamic efficiency occurred at 4°-6° angle of attack for all airfoils. NACA 4412 maintained superior performance across the tested range, with Eppler and Clark Y showing comparable but slightly reduced efficiency.

5.2.4 Lift Coefficient (C_L) vs Drag Coefficient (C_D)

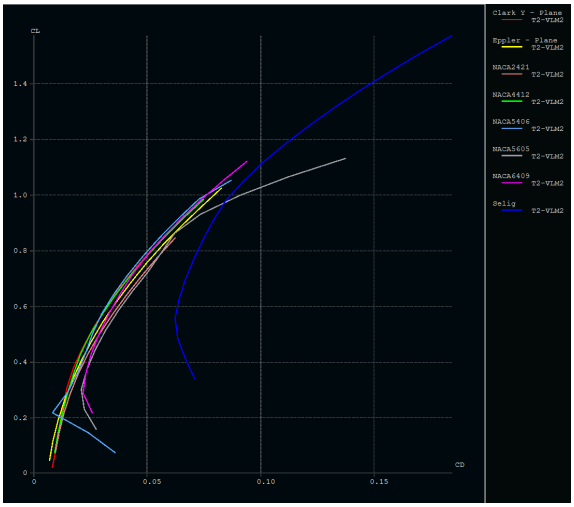

Figure 10: Air: Lift coefficient (C_L) vs. drag coefficient (C_D)

NACA 4412 demonstrated the most favorable polar curve, achieving higher lift with minimal drag penalty. Eppler and Clark Y showed similar but less pronounced performance advantages, while Selig 1223 exhibited the poorest lift-drag relationship.

5.2.5 Forward Velocity (V_X) vs Angle of Attack (α)

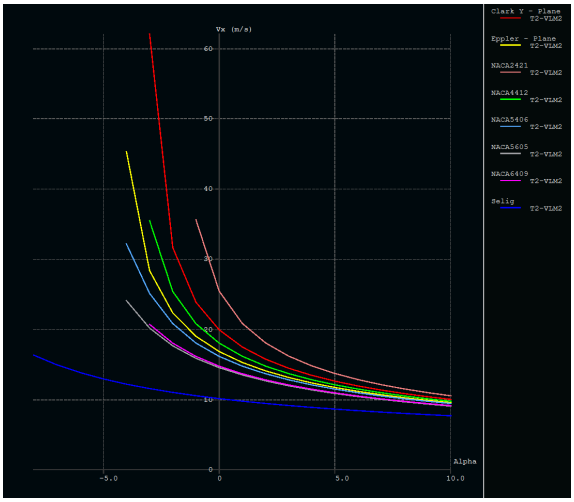

Figure 11: Air: Cruise velocity (V_x) vs. angle of attack (α)

NACA 4412 and Eppler maintained stable velocity characteristics up to 8° angle of attack, while Selig 1223 showed significant velocity degradation beyond 5° due to increased drag effects.

5.2.6 Drag Coefficient (C_D) vs Velocity (V_X)

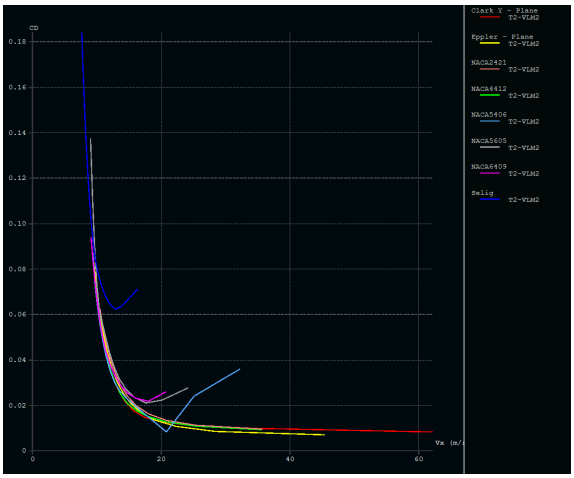

Figure 12: Air: Drag coefficient (C_D) vs. cruise velocity (V_x)

The lowest drag coefficients were observed for NACA 4412 and Eppler across the velocity spectrum. Clark Y showed moderate performance, with Selig 1223 exhibiting substantially higher C_D values, particularly at velocities above $10m/s$.

5.2.7 Lift Coefficient (C_L) vs Angle of Attack (α)

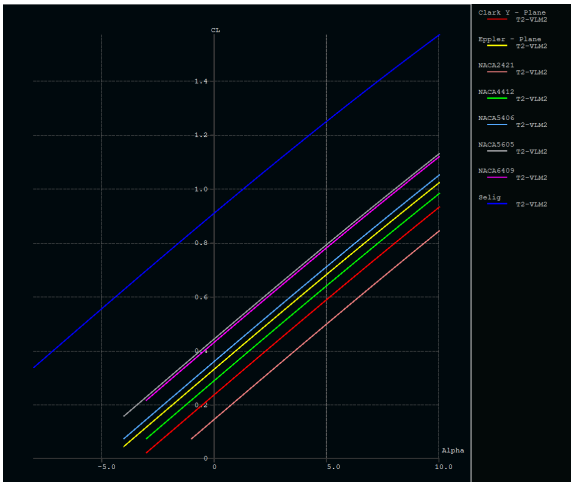

Figure 13: Air: Lift coefficient (C_L) vs. angle of attack (α)

The NACA 4412 showed the highest maximum lift coefficient with gradual stall, while Eppler and Clark Y had moderate but stable lift, and Selig 1223 exhibited aggressive lift increase followed by abrupt stall.

5.2.8 Drag Coefficient (C_D) vs Angle of Attack (α)

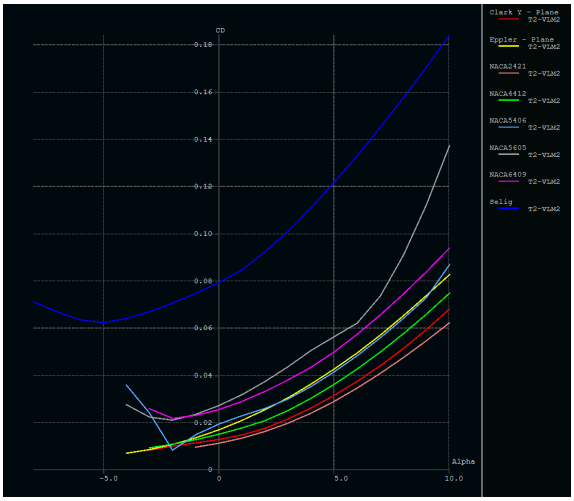

Figure 14: Air: Drag coefficient (C_D) vs. angle of attack (α)

NACA 4412 and Eppler maintained the lowest drag coefficients across all tested angles. Clark Y showed acceptable performance, while Selig 1223 exhibited rapid drag increase beyond 6° angle of attack.

5.2.9 Summary

- Cruise velocity: 15 m/s (optimal aerodynamic efficiency)
- Thrust requirement: 1.2 N (minimum drag conditions)

5.3 Wing Hydrodynamic Performance in Water

5.3.1 Drag Force (F_X) vs Velocity (V_X)

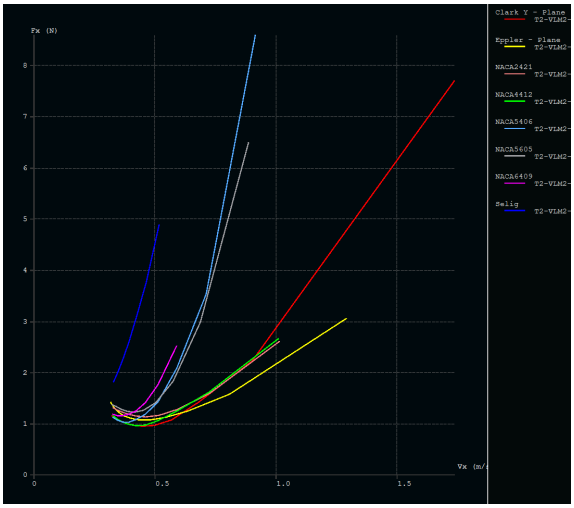

Figure 15: Water: Drag force (F_x) vs. cruise velocity (V_x)

NACA 4412, Clark Y, and Eppler showed minimal drag across 0.2-0.8 m/s, with optimal performance at 0.5 m/s. Selig 1223 exhibited substantially higher drag, especially at higher velocities.

5.3.2 Lift-to-Drag Ratio (C_L/C_D) vs Lift Coefficient (C_L)

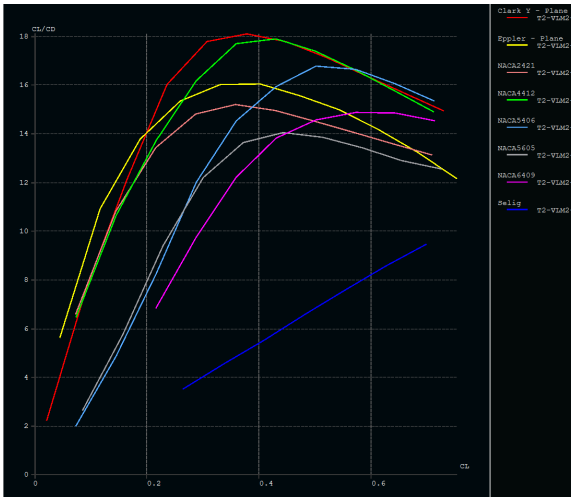

Figure 16: Water: Lift-to-drag ratio (C_L/C_D) vs. lift coefficient (C_L)

NACA 4412 and Eppler achieved peak C_L/C_D of 18 at moderate lift coefficients. Clark Y performed slightly worse, while Selig 1223 showed significantly lower efficiency across all conditions.

5.3.3 Lift-to-Drag Ratio (C_L/C_D) vs Angle of Attack (α)

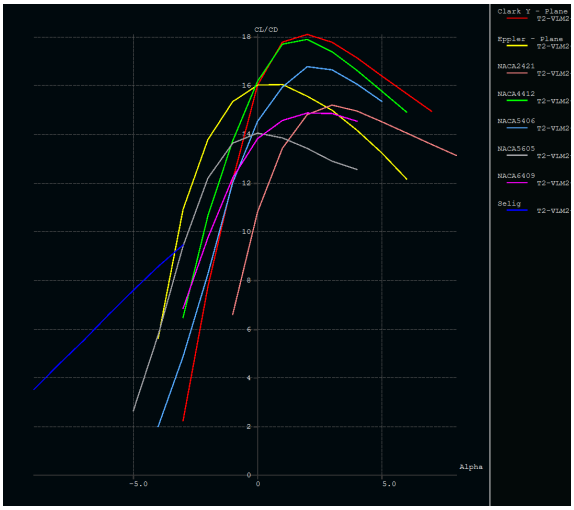

Figure 17: Water: Lift-to-drag ratio (C_L/C_D) vs. angle of attack (α)

Maximum efficiency occurred at 4°-6° AoA. NACA 4412 maintained superior performance across the tested range, while Selig 1223 showed early efficiency degradation.

5.3.4 Lift Coefficient (C_L) vs Drag Coefficient (C_D)

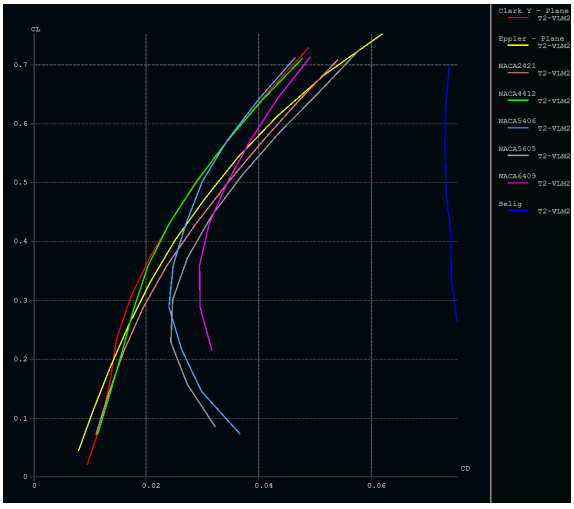

Figure 18: Water: Lift coefficient (C_L) vs. drag coefficient (C_D)

NACA 4412 demonstrated optimal performance with high lift and minimal drag. Eppler and Clark Y followed closely, while Selig 1223 required substantially more drag for equivalent lift.

5.3.5 Forward Velocity (V_X) vs Angle of Attack (α)

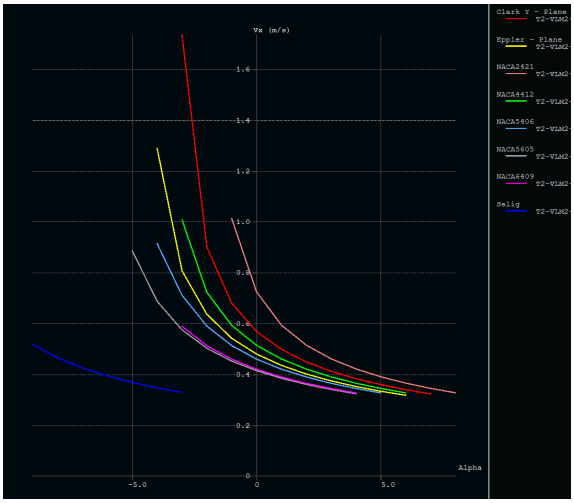

Figure 19: Water: Cruise velocity (V_x) vs. angle of attack (α)

NACA 4412 and Eppler maintained stable velocities up to 8° AoA. Selig 1223 showed significant speed reduction at higher angles due to increased drag.

5.3.6 Drag Coefficient (C_D) vs Velocity (V_X)

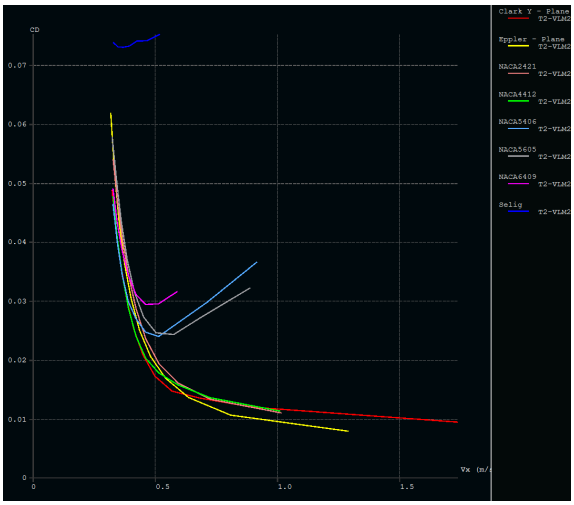

Figure 20: Water: Drag coefficient (C_D) vs. cruise velocity (V_x)

NACA 4412 and Eppler maintained the lowest drag coefficients across all velocities. Selig 1223 showed velocity-sensitive drag characteristics with substantially higher values.

5.3.7 Lift Coefficient (C_L) vs Angle of Attack (α)

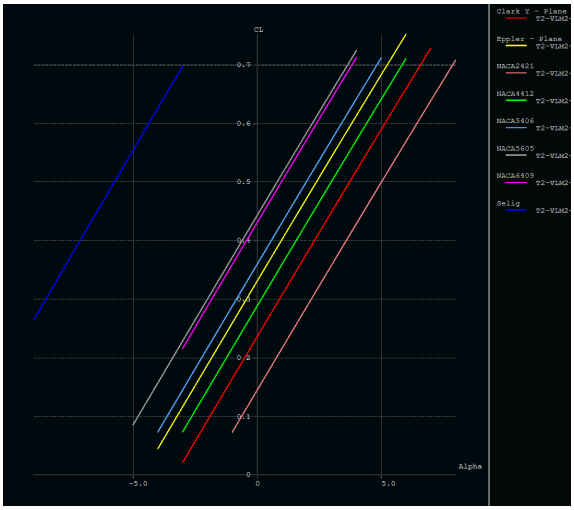

Figure 21: Water: Lift coefficient (C_L) vs. angle of attack (α)

NACA 4412 achieved the highest maximum lift with gradual stall. Eppler and Clark Y showed stable performance, while Selig 1223 exhibited abrupt stall behavior.

5.3.8 Drag Coefficient (C_D) vs Angle of Attack (α)

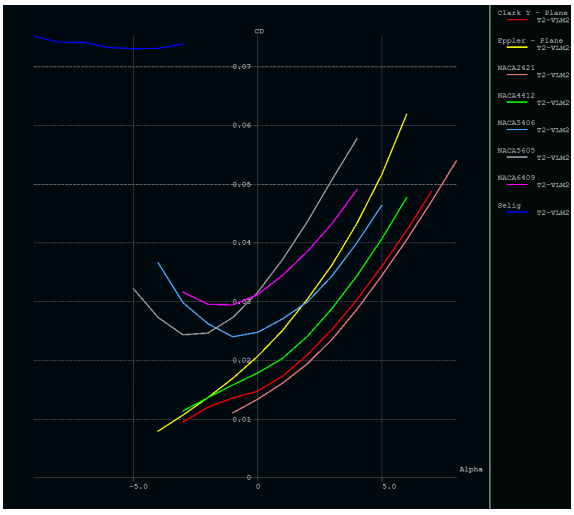

Figure 22: Water: Drag coefficient (C_D) vs. angle of attack (α)

NACA 4412 maintained the lowest drag across all angles. Selig 1223 showed rapid drag increase at higher angles, indicating flow separation issues.

5.3.9 Summary

- Cruise velocity: 0.5 m/s (optimal aerodynamic efficiency)
- Thrust requirement: 1 N (minimum drag conditions)

6 Propeller Aerodynamic and Propulsive Analysis

6.1 Initial Assumptions and Parameters

The following assumptions and parameters were considered for the analysis:

- **Propeller Configuration**: Generic two-bladed propeller.
- **Geometry**:
  - Number of blades: $N = 2$
  - Blade chord: $C = 0.2$ m
  - Propeller diameter: $D = 0.26$ m
  - Radius: $R = D/2 = 0.13$ m
- **Operating Conditions**:
  - In water: $V_{\text{water}} = 0.5$ m/s
  - In air: $V_{\text{air}} = 15$ m/s
- **Thrust Requirements**:
  - Thrust in water: $T_{\text{water}} = 1$ N
  - Thrust in air: $T_{\text{air}} = 1.2$ N
- **Fluid Properties**:
  - Water density: $\rho_{\text{water}} = 1000$ kg/m^3
  - Air density: $\rho_{\text{air}} = 1.225$ kg/m^3

The blade geometry at various radial stations is summarized below:

r/R	c/R	β (degrees)
0.15	0.138	37.86
0.20	0.154	45.82
0.25	0.175	44.19
0.30	0.190	38.35
0.35	0.198	33.64
0.40	0.202	29.90
0.45	0.200	27.02
0.50	0.195	24.67
0.55	0.186	22.62
0.60	0.174	20.88
0.65	0.161	19.36
0.70	0.145	17.98
0.75	0.129	16.74
0.80	0.112	15.79
0.85	0.096	14.64
0.90	0.081	13.86
0.95	0.061	12.72
1.00	0.040	11.53

Table 2: Blade Geometry at Various Radial Stations

6.2 Propeller Performance in Air

6.2.1 Solidity Ratio (σ)

The solidity ratio is calculated as:

$$\sigma = \frac{NC}{\pi R}$$

Substituting the given values:

$$\sigma = \frac{2 \times 0.2}{\pi \times 0.13} = 0.13$$

6.2.2 Thrust Coefficient (C_T)

Given:

$$\frac{C_T}{\sigma} = 0.1$$

Thus:

$$C_T = 0.1 \times 0.13 = 0.013$$

6.2.3 Propeller Rotational Speed (n_{air})

Using the thrust relation:

$$n_{\text{air}} = \sqrt{\frac{T_{\text{air}}}{C_T \rho_{\text{air}} D^4}}$$

Substituting:

$$n_{\text{air}} = \sqrt{\frac{1.2}{0.013 \times 1.225 \times (0.26)^4}} = 128.41\,\text{RPS}$$

In RPM:

$$n_{\text{air}} = 128.41 \times 60 = 7704.7\,\text{RPM}$$

6.2.4 Advance Ratio (J_{air})

$$J_{\text{air}} = \frac{V_{\text{air}}}{n_{\text{air}} D} = \frac{15}{128.41 \times 0.26} = 0.449$$

6.3 Propeller Performance in Water

6.3.1 Thrust Coefficient (C_T)

The thrust coefficient remains unchanged:

$$C_T = 0.013$$

6.3.2 Propeller Rotational Speed (n_{water})

$$n_{\text{water}} = \sqrt{\frac{T_{\text{water}}}{C_T \rho_{\text{water}} D^4}}$$

Substituting:

$$n_{\text{water}} = \sqrt{\frac{1}{0.013 \times 1000 \times (0.26)^4}} = 12.97\,\text{RPS}$$

In RPM:

$$n_{\text{water}} = 12.97 \times 60 = 778.45\,\text{RPM}$$

6.3.3 Advance Ratio (J_{water})

$$J_{\text{water}} = \frac{V_{\text{water}}}{n_{\text{water}} D} = \frac{0.5}{12.97 \times 0.26} = 0.148$$

6.4 Propeller Performance Curves

The non-dimensional performance characteristics are shown in Figure 23.

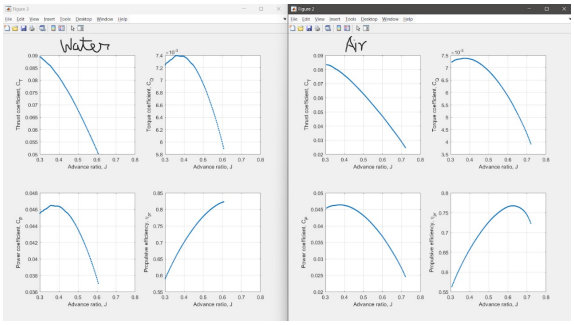

Figure 23: Performance curves for propeller operation in air and water.

7 Propeller Redesign and Reanalysis (Analysis 2)

7.1 Blade Geometry Modification

The initial analysis revealed a significant disparity between the advance ratios in air and water. To achieve better dual-medium performance, the blade pitch angle β was reduced by approximately 10° across all radial stations while maintaining the chord distribution.

The updated blade geometry is:

r/R	c/R	β (degrees)
0.15	0.138	27.86
0.20	0.154	35.82
0.25	0.175	34.19
0.30	0.190	28.35
0.35	0.198	23.64
0.40	0.202	19.90
0.45	0.200	17.02
0.50	0.195	14.67
0.55	0.186	12.62
0.60	0.174	10.88
0.65	0.161	9.36
0.70	0.145	7.98
0.75	0.129	6.74
0.80	0.112	5.79
0.85	0.096	4.64
0.90	0.081	3.86
0.95	0.061	2.72
1.00	0.040	1.53

Table 3: Updated Blade Geometry after Pitch Reduction

7.2 Methodology for Determining Required Rotational Speed

The thrust is given by:

$$T = \rho n^2 D^4 C_T(J)$$

where $J = \frac{V}{nD}$.

The thrust coefficient $C_T(J)$ was modeled as a polynomial:

In Air:

$$C_T(J) = -0.2219J^4 + 0.733J^3 - 0.7861J^2 + 0.1428J + 0.04298$$

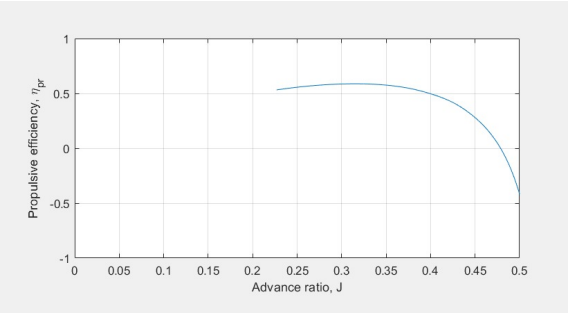

Figure 24: Variation of propulsion efficiency (η_{pr}) with advanced ratio (J) in air

In Water:

$$C_T(J) = -0.9574J^4 + 2.094J^3 - 1.741J^2 + 0.4238J + 0.01544$$

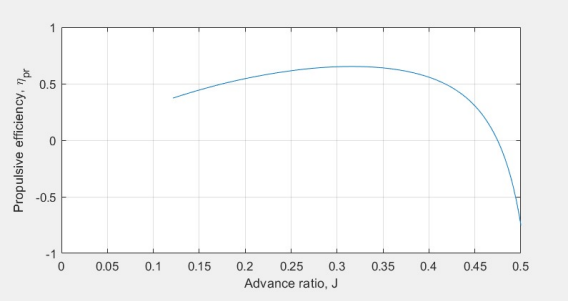

Figure 25: Variation of propulsion efficiency (η_{pr}) with advanced ratio (J) in water

The equations were solved using MATLAB's `fzero` function.

7.3 Results

- **In Air**:

$$n_{\text{air}} = 136.93\,\text{RPS} \quad \text{or} \quad 8216.01\,\text{RPM}$$

$$J_{\text{air}} = 0.421$$

- **In Water**:

$$n_{\text{water}} = 4.53\,\text{RPS} \quad \text{or} \quad 271.79\,\text{RPM}$$

$$J_{\text{water}} = 0.425$$

7.4 Conclusion

The redesigned propeller blade resulted in advance ratios:

$$J_{\text{air}} = 0.421, \quad J_{\text{water}} = 0.425$$

The close match indicates a significant improvement in dual-medium efficiency.

8 Results and Conclusions

8.1 Airfoil Performance Analysis

Aerodynamic analyses were conducted for five airfoil profiles: Eppler, Selig 1223, Clark Y, NACA 4412, and NACA 2421, evaluated across Reynolds numbers ranging from 3×10^5 to 1×10^6.

8.1.1 Lift and Drag Characteristics

The NACA 4412 airfoil demonstrated the highest maximum lift coefficient ($C_{L,\max} \approx 1.5$) with a smooth stall onset. Eppler E197 maintained stable lift (C_L) across wide angles of attack. Selig 1223, despite achieving early lift, exhibited sharp stall at angles beyond 10°.

8.1.2 Aerodynamic Efficiency

The lift-to-drag ratio (C_L/C_D) peaked between 4° and 6° angles of attack for all airfoils. Eppler achieved the highest C_L/C_D value of approximately 22, followed closely by NACA 4412 ($C_L/C_D \approx 21$) and Clark Y ($C_L/C_D \approx 20$).

8.2 Wing Performance Analysis in Air

8.2.1 Drag and Lift-to-Drag Behavior

The designed wing using NACA 4412 profile exhibited minimum drag force of approximately 1.2 N at a cruise velocity of 15 m/s. Lift-to-drag ratios achieved maximum values near $C_L \approx 0.5$ with corresponding C_L/C_D around 22.

8.2.2 Velocity and Stall Characteristics

At an angle of attack of 6°, the wing achieved optimal cruise conditions, with stable lift and minimum drag characteristics. Beyond 8°, a gradual decrease in aerodynamic performance was observed.

8.3 Wing Performance Analysis in Water

8.3.1 Drag and Efficiency in Water

In waterborne conditions, optimal cruise occurred at approximately 0.5 m/s, where drag forces were minimized to around 1.0 N. NACA 4412 exhibited the best hydrodynamic lift-to-drag ratio, achieving $C_L/C_D \approx 18$ at moderate angles of attack (4°–6°).

8.4 Propeller Analysis

8.4.1 Baseline Propeller Design

The initial two-blade propeller ($D = 0.26$ m, $C = 0.2$ m) required:

- In Air: $n_{\text{air}} = 7704.7$ RPM to generate $T_{\text{air}} = 1.2$ N.
- In Water: $n_{\text{water}} = 778.45$ RPM to generate $T_{\text{water}} = 1.0$ N.

The initial advance ratios were $J_{\text{air}} = 0.449$ and $J_{\text{water}} = 0.148$, indicating inefficiencies.

8.4.2 Blade Geometry Optimization

After reducing the pitch angle β by approximately 10° at all radial stations:

- Optimized Advance Ratios achieved: $J_{\text{air}} = 0.421$ and $J_{\text{water}} = 0.425$.
- New Rotational Speeds: $n_{\text{air}} = 8216$ RPM and $n_{\text{water}} = 271.8$ RPM.

The advance ratios became nearly equal, ensuring optimal thrust generation in both media.

8.5 Final Conclusions

- **Best Performing Airfoil**: NACA 4412, with $C_{L,\max} \approx 1.5$ and maximum $C_L/C_D \approx 22$.
- **Optimal Wing Operating Points**:
  - Airborne Cruise: 15 m/s, Thrust ≈ 1.2 N.
  - Waterborne Cruise: 0.5 m/s, Thrust ≈ 1.0 N.
- **Propeller Performance**: After optimization, J_{air} and J_{water} matched closely, with $\Delta J \approx 0.004$.
- **Overall Outcome**: The design meets amphibious operational requirements with efficient airfoil, wing, and propeller configurations, enabling smooth transition between water and air.

Future extensions include experimental validations, further propeller refinement, and incorporation of hull water spray analysis during transition phases.

References

[1] Andy Lennon, *Basics of R/C Model Aircraft Design*, 1996.
https://pdfcoffee.com/basics-of-rc-model-aircraft-design-2-pdf-free.html

[2] Or Dantsker et. al., *Performance Testing of APC Electric Fixed-Blade UAV Propellers*, 2022.
https://www.researchgate.net/publication/361456490_Performance_Testing_of_APC_Electric_Fixed-Blade_UAV_Propellers

[3] Sumeet Kumar, *Fundamentals of Helicopter Aerodynamics*, 2021.
https://kumar-sumeet.github.io/HeliAeroNotes/Opening.html

[4] *Blade Element Momentum Theory (BEMT)*, 2019
https://github.com/cotri/BEMT/tree/master